Zitierweise: *Angew. Chem. Int. Ed.* **2025**, *64*, e202414981
doi.org/10.1002/anie.202414981

Metabolic Engineering

A photosynthesis-derived bionic system for sustainable biosynthesis

Na Chen[+], Ruichen Shen[+], Tianpei He[+], Jing Xi, Rui Zhao, Na Du, Yangbing Yang, Lilei Yu, and Quan Yuan**

Abstract: "Cell factory" strategy based on microbial anabolism pathways offers an intriguing alternative to relieve the dependence on fossil fuels, which are recognized as the main sources of CO_2 emission. Typically, anabolism of intracellular substance in cell factory requires the consumption of sufficient reduced nicotinamide adenine dinucleotide /nicotinamide adenine dinucleotide phosphate NAD(P)H and adenosine triphosphate ATP. However, it is of great challenge to modify the natural limited anabolism and to increase the insufficient level of NAD(P)H and ATP to optimum concentrations without causing metabolic disorder. Inspired by the natural photosynthesis process in which NAD(P)H and ATP can both be produced through the coupled electron-proton transfer processes driven by sunlight, herein we designed a light-driven bionic system composed of three modules including photo-induced electron module, electron transfer channel module and proton gradient module. The proposed strategy of light-driven bionic system enables for achieving simultaneous and controllable supplies of NAD(P)H and ATP, thus facilitating both highly efficient CO_2 fixation and biomanufacturing. The proposed light-driven bionic system design strategy in this work might pave new sustainable ways for reducing power and energy regeneration to optimize microbial metabolism, offering intriguing alternatives for CO_2 emission mitigation and high-value chemical biomanufacturing.

Introduction

Climate change caused by massive CO_2 emission impacts on worldwide economic and environmental sustainability and has currently drawn tremendous attentions.[1] The ambitious target for CO_2 emission reduction has been on the global agenda and imminently calls for green and sustainable industrial approaches.[2] Microbes, which permeate virtually on the every corner of earth, have evolved a variety of metabolic pathways, such as Calvin cycle for CO_2 fixation, and are widely recognized to play key roles in early CO_2-domainated atmosphere evolution.[3] Additionally, with their abundant and specific metabolic pathways, microbes are capable of acting as factories for converting CO_2 into highly value-added long chain chemicals under mild conditions.[4] This "cell factory" strategy offers an intriguing alternative for the chemical productions, relieving the dependence on fossil fuels which are recognized as the main sources of CO_2 emission.[5] To this end, researchers are striving to "open source and reduce expenditure" for the mitigation of CO_2 emissions and the efficient biosynthesis of value-added chemicals.

Typically, anabolism in "cell factory" such as CO_2 fixation and biosynthesis, requires the consumption of sufficient reducing equivalents and energy. The reduced nicotinamide adenine dinucleotide /nicotinamide adenine dinucleotide phosphate NAD(P)H and adenosine triphosphate (ATP) are widely recognized as the key reducing power and critical energy "currency" respectively in cells.[6] However, microbes have genetically evolved to survive rather than to produce value-added chemicals, and the deficiency in intracellular equivalents of NAD(P)H and ATP hinders the practical applications in both CO_2 fixation and biomanufacturing.[7] Interventions targeting pathways associated with NAD(P)H and ATP, such as the pentose phosphate pathway and the tricarboxylic acid (TCA) cycle hold promise in supplying the critical reducing equivalents and energy.[6b] However, the directed interventions of the critical pathways through genetic operations always lead to cellular metabolic disorder among the complex metabolic network.[6b] Therefore, construction of NAD(P)H and ATP self-supply system without causing metabolic disorder and is essential to enhance cellular anabolism.

In nature, photosynthesis drives NADPH and ATP production with light as the source of energy, PSI/PSII photosystems as the energy converter, and electrons flowing through membrane and soluble proteins.[6b,8] Specifically, photosynthetic pigments harvest the sunlight and induce proton-coupled electron transfer.[8a] Electrons then drive the NADPH production via the electron transfer chain, and the proton gradient derived from the free energy of the electron transfer reactions drives the ATP synthesis.[8a] Therefore, developing an NADPH and ATP self-supply system, which

[*] N. Chen,[+] T. He,[+] J. Xi, R. Zhao, N. Du, Y. Yang, L. Yu, Q. Yuan
Renmin Hospital of Wuhan University, College of Chemistry and Molecular Sciences, Institute of Molecular Medicine, School of Microelectronics
Wuhan University, Wuhan 430072, P. R. China
E-mail: yuanquan@whu.edu.cn
lileiyu@whu.edu.cn

R. Shen,[+] Q. Yuan
Molecular Science and Biomedicine Laboratory (MBL), State Key Laboratory of Chemo/Biosensing and Chemometrics College of Chemistry and Chemical Engineering
Hunan University, Changsha 410082, P. R. China

[+] These authors contributed equally to this work.

emulates the natural process of NADPH and ATP production during photosynthesis, presents a promising approach for achieving highly efficient anabolic processes such as CO_2 fixation and biosynthesis within cellular factories.

Inspired by the natural photosynthesis process, herein we designed a controllable light-driven bionic system composed of three modules, including a photo-induced electron module, an electron transfer channel module and a proton gradient module, for the simultaneous and controllable supply of NADPH and ATP, achieving both highly efficient CO_2 fixation and biomanufacturing. To be specific, as shown in Figure 1, the photo-induced electron module was achieved by regulating lattice defects and energy levels in the photocatalyst model of $Zn_{1.2}Ga_{1.6}Ge_{0.2}O_4$:Ni (ZGGO:Ni) to generate both photo-induced electrons with high charge separation efficiency and electron carrier hydrogen, driving for the generation of reducing power NADPH. The electron transfer channel module was obtained by constructing a polydopamine (PDA) coating with conjugated π structure, possessing excellent electron transport and adhesion abilities. The module optimizes the electron transfer kinetics and physical interface between ZGGO:Ni and the microorganism, decreasing the internal and external electron transfer resistance and improving electron utilization efficiency. Finally, the proton gradient module was established by adopting the coupled electron-proton transfer processes to generate light-driven ATP. Additionally, anchoring H^+ pumping proteorhodopsin could further drives a proton gradient to supply ATP. By synergistically integrating these three key modules under light exposure, the anabolic efficiencies including both CO_2 fixation and lycopene biosynthesis in *Rhodopseudomonas palustris* (*R. palustris*) model are significantly enhanced. The results indicate that the enhanced efficiency is due to the strategic supplementation of critical reducing equivalents and energy, which had been previously identified as limiting factors. This proposed light-driven bionic system achieves an electron transfer efficiency up to 90.8 %, approaching to the limiting value. Furthermore, the integration of the light-driven bionic system results in a 1.6-fold increase in the apparent photo conversion efficiency (APCE), showcasing a significant enhancement in energy utilization. We anticipate our demonstration as a pioneering step towards NAD(P)H and ATP self-supply by harnessing the boundless potential of sustainable solar energy, paving new ways for transformative revolution in manufacturing industry.

Results and Discussion

Analogous to PSI/PSII photosystems in natural photosynthesis, semiconductor nanomaterials also have the ability to convert solar energy into reducing equivalents.[9] It merits emphasis that defects within nanomaterials can suppress the recombination of photo-excited electrons and provide conduits for electron migration, thereby enhancing the electron transfer efficiency towards microorganisms.[7a] Moreover, the utilization of semiconductors featuring an appropriate band structure facilitates photocatalytic water splitting. This process effectively stores electrons in the form of hydrogen,

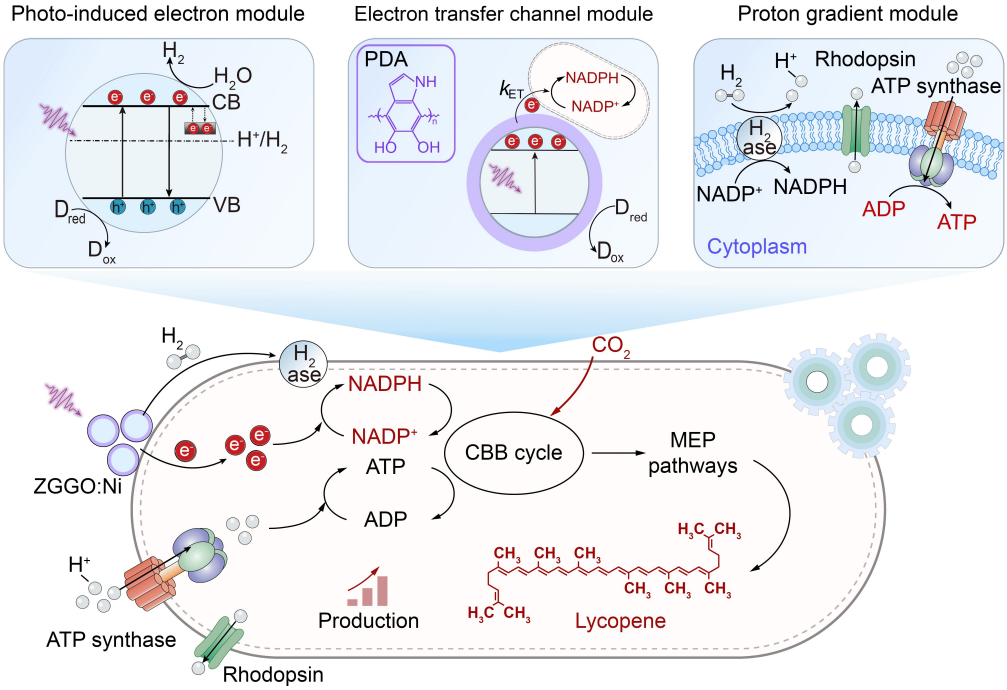

Figure 1. Schematic illustration of light-driven bionic system consisting of the photo-induced electron module, electron transfer channel module and proton gradient module driving microbial anabolism. The designed bionic system drives the simultaneous and controllable supply of NADPH and ATP, achieving both highly efficient CO_2 fixation and biomanufacturing. D_{red}, electron donors in the cell culture medium; D_{ox}, oxidized electron donor species; CB, conduction band; VB, valance band.

thereby providing a conduit for the essential delivery of reducing equivalents to microbes.[10] Consequently, by employing a strategy that involves defect regulation and band structure engineering, we have meticulously designed the photo-induced electron module to enhance its overall performance. As a proof of concept, we strategically introduced oxygen vacancy defects into ZGGO:Ni, aligning the energy levels to enhance charge separation and promote hydrogen evolution. This approach ensures an efficient supply of photo-induced electrons, which are essential for driving the generation of NADPH in microbes.

Subsequently, photo-induced electrons or electron carrier H_2 acting as the sources of reducing equivalents can be delivered into microbes for NADPH generation. However, the sluggish biotic/abiotic interfacial electron exchange between the semiconductor and microbe largely limits the reducing equivalent NADPH generation performance and practical biomanufacturing processes.[11] To circumvent this problem, photocatalyst nanoparticle was encapsulated by in situ polymerization within a π-conjugated PDA layer, acting as an electron transfer mediator from ZGGO:Ni towards the microbes. The PDA′s delocalized electron transmission channel facilitates a reduction in exciton binding energy and expedites the internal charge transfer process, thereby enhancing electron transfer efficiency from ZGGO:Ni towards microbes.[12] In addition, PDA's excellent adhesion ability allows ZGGO:Ni to bind to the surface of microorganism through electrostastic interactions, benefiting the electron transfer across the semiconductor-microbe interfaces.[13]

Similar to the natural photosynthesis, the electron transfer chain subsequently couples the redox reactions to proton translocation to build up a proton motive force across the membrane, which in turn drives ATP synthesis.[14] In addition, the electron carrier H_2 from the light-driven photo-induced electron module also enables further proton translocation by H_2 oxidation via the hydrogenase on the membrane of microbes to fuel ATP synthesis.[14] Furthermore, we have incorporated proteorhodopsin, a light-harvesting molecule capable of generating a proton motive force, to facilitate ATP synthesis upon light capture. In summary, our rational design of a light-driven bionic system offers innovative solutions for the simultaneous and controllable supply of NADPH and ATP, paving the ways for highly efficient CO_2 fixation and biomanufacturing.

To provide microbes with a source of reducing power, we have carefully crafted the photo-induced electron module, leveraging strategies of defect regulation and band structure engineering. ZGGO:Ni with appropriate energy levels and long-lived electrons was selected as the model of the photo-induced electron module (Figure S1). Firstly, theoretical simulations were performed by the Vienna ab initio simulations package using the projector-augmented wave method to determine how the defects influence the behaviors of photo-induced electrons. Figure 2a shows the charge distribution imaged by the DFT calculation with electron-rich and electron-deficient regions indicated in red and blue, respectively. It can be clearly observed that the charge density around an oxygen vacancy (V_O, using Kröger-Vink notations) in the photo-induced electron module of ZGGO:Ni decreases, indicating a very local influence on the host material arising from the oxygen vacancies (Table S1). The decreased electron charge density around the oxygen vacancies leads to positive local charges, which is beneficial for the capture of photo-induced electrons and facilitates the charge separation. In addition, ZGGO:Ni with appropriate energy levels theoretically enables hydrogen evolution (Figure S2). Further insight into the potential influences of oxygen vacancies on hydrogen evolution, water absorption, water dissociation and hydrogen desorption processes with ZGGO:Ni, was obtained by calculating the corresponding Gibbs free energy (ΔG). As shown in Figure 2b, all the ΔG values of different stages are more negative upon introducing oxygen vacancies. Notably, during the water absorption and hydrogen desorption processes, the Gibbs free energy of ZGGO:Ni are –26.22 kJ/mol and 43.79 kJ/mol, while the values of ZGGO:Ni with oxygen vacancies are –53.36 kJ/mol and –16.45 kJ/mol respectively. The theoretical results indicate that the oxygen vacancies are energetically favorable for the hydrogen evolution reactions (HER).

Subsequently, ZGGO:Ni with rich oxygen vacancies (R-ZGGO:Ni) and poor oxygen vacancies (P-ZGGO:Ni) were prepared by defect engineering via calcination under an inert atmosphere and O_2 atmosphere, respectively[15] (Figure S3). The low temperature electron paramagnetic resonance (EPR) spectra in Figure 2c clearly shows paramagnetic centers formed in ZGGO:Ni. According to a previous report,[16] g-factors at 2.00 can be assigned to electrons trapped in V_O. It can be observed that the EPR intensity increased in R-ZGGO:Ni samples, further validating the successful introduction of oxygen vacancies into ZGGO:Ni.[16] In transient photocurrent tests, R-ZGGO:Ni produced a cathodic photocurrent 2.0 times higher than that of P-ZGGO:Ni, demonstrating that oxygen vacancies promote the electron-donating ability (Figure 2d). Overall, the above results demonstrate that oxygen vacancies efficiently facilitate charge separation (Figure S4). Furthermore, photocatalytic H_2 evolution tests were performed to determine the electron donating ability of the designed light-driven photo-induced module. Figure 2e shows that R-ZGGO:Ni achieves 1.3 times higher HER rates compared to P-ZGGO:Ni. In line with theoretical expectations, the elevated hydrogen evolution rate (HER) of R-ZGGO:Ni is primarily due to the oxygen vacancies that promote efficient charge separation and reduce the activation energy (Table S2). These experimental findings further corroborate that our light-driven photo-induced module, strategically designed through defect regulation and band structure engineering, effectively supplies electrons and electron carriers as reducing power sources.

To ascertain the photo-induced module's capacity to facilitate the generation of NADPH reducing equivalents in microbes, $NADP^+$ reduction tests were performed in vitro. As depicted in Figure 2f, the characteristic absorbance peak of NADPH at 340 nm is evident under light irradiation with R-ZGGO:Ni alone, whereas it is negligible in the dark conditions. This distinct difference indicates that the R-

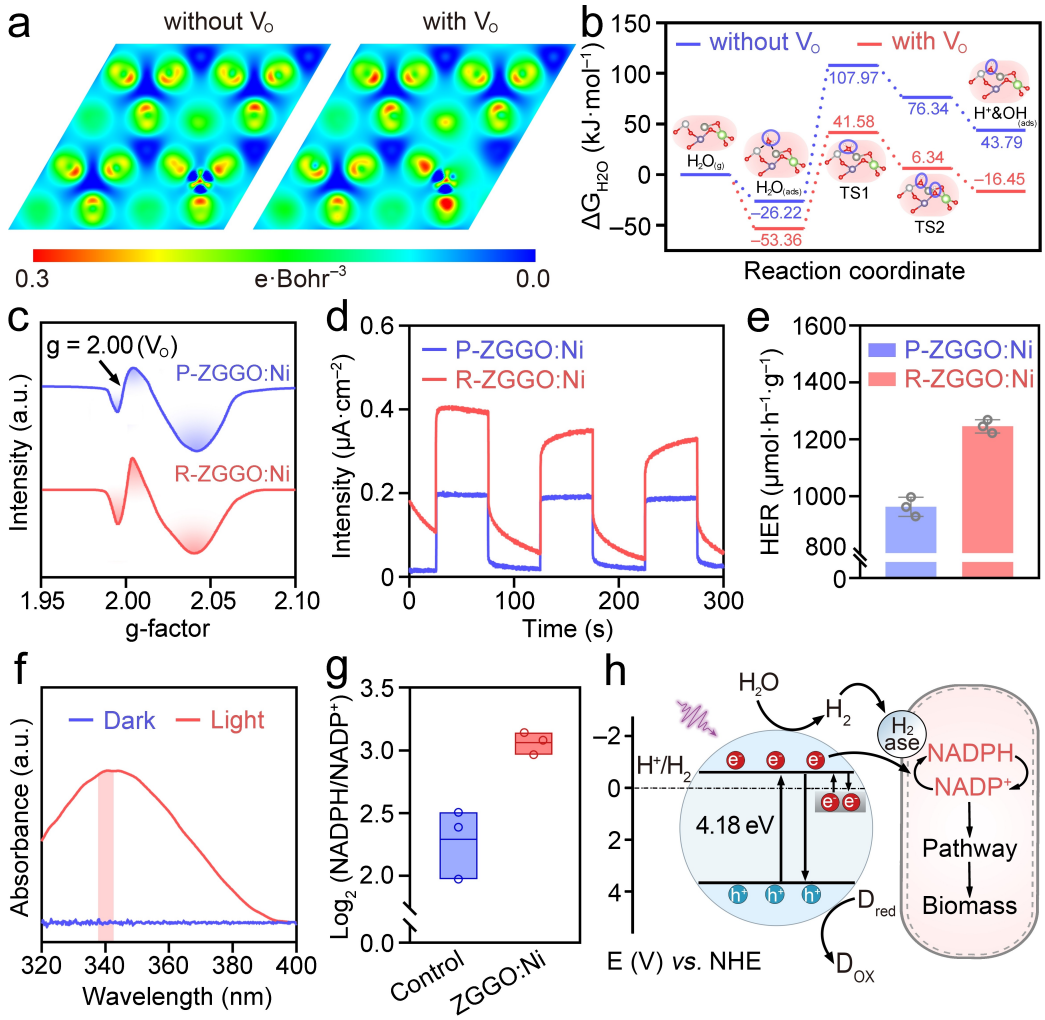

Figure 2. Photo-induced module drives the generation of NADPH. (a) 2D differential charge density diagrams of ZGGO:Ni. (b) Free energy versus the reaction coordinates of HER for different active sites (Blue for ZGGO:Ni without oxygen vacancies and red for ZGGO:Ni with oxygen vacancies). The insets are the corresponding reactive intermediate models. (c) EPR spectra of P-ZGGO:Ni and R-ZGGO:Ni. (d) Photocurrent responses under 300 W Xenon lamp illumination. (e) H_2 evolution rate (HER) of P-ZGGO:Ni and R-ZGGO:Ni. Data presented as mean values ± SD., $n = 3$. f, Absorbance of the NADPH produced under different conditions. (g) Log_2 (NADPH/NADP$^+$) in *R. palustris*. Data presented as mean values ± SD., $n = 3$. (h) Schematic illustration of photo-induced electron module driving NADPH generation.

ZGGO:Ni photo-induced module enables for the generation of essential NADPH reducing equivalents.[7a,17] *R. palustris*, a purple nonsulfur bacterial species, is selected as a research model for its ability to produce the high-value chemical lycopene via the methylerythritol 4-phosphate (MEP) pathways and to fix CO_2 through the Calvin-Benson-Bassham (CBB) cycle. Figure 2g demonstrates that the log_2 (NADPH/NADP$^+$) value in *R. palustris* model with the addition of R-ZGGO:Ni is 1.34 times higher than that in bare *R. palustris*, further validating that the photo-induced module drives NADPH generation. The increased NADPH/NADP$^+$ ratio in *R. palustris* model can be attributed to the direct photo-induced electron transfer and the indirect H_2-mediated electron transfer. In summary, the outcomes underscore that our strategic design of the photo-induced module, grounded in defect regulation and band structure engineering, yields novel insights into the generation of vital NADPH reducing equivalents (Figure 2h). This approach advances our understanding of light-driven bioenergetics and holds promise for innovative applications in biomanufacturing.

The reducing power including electrons and electron carriers from the photo-induced module enables driving NADPH generation in *R. palustris* microbe. However, the transfer of reducing energy to organic living systems is confronted with internal and external electron transfer resistances, leading to an extremely low electron utilization efficiency in microorganisms.[11b] An interface with low electron transfer resistance is critical in facilitating reducing power transfer into microbes.[11b] Here, electron transfer channel module to bridge the photo-induced module and microbes was constructed by encapsulating PDA with excellent adhesion and electron transport capabilities (Figure S5). Electrochemical impedance spectroscopy (EIS) analysis in Figure 3a reveals that by encapsulating the PDA, the charge transfer resistance decreases, suggesting

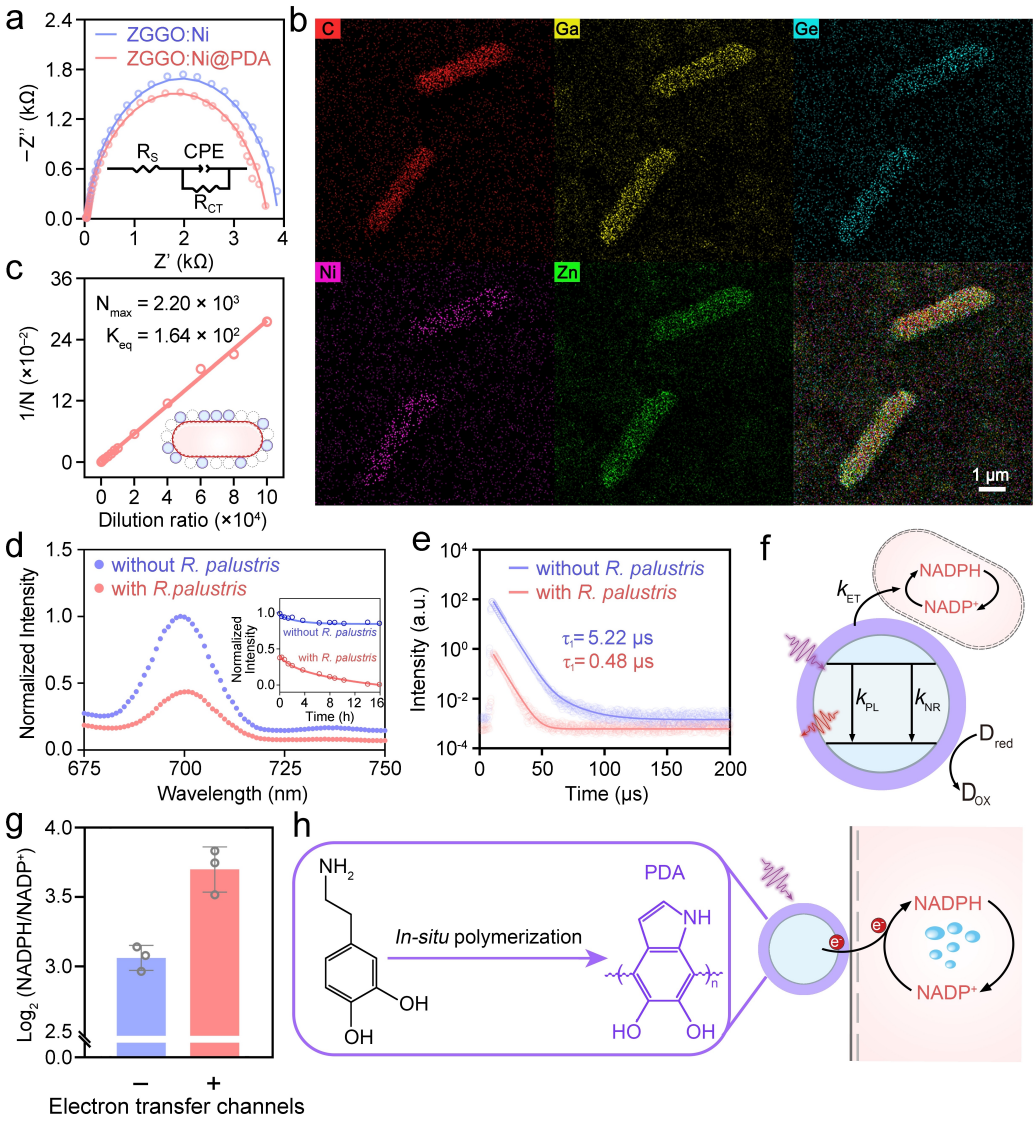

Figure 3. Electron transfer channels promote interfacial charge-transfer kinetics. (a) Electrochemical impedance spectroscopy (EIS) curves of ZGGO:Ni (blue) and ZGGO:Ni@PDA (red) electrodes. (b) SEM-EDX elemental mapping images of *R. palustris*-ZGGO:Ni@PDA. (c) Plot of 1/N versus dilution ratio of ZGGO:Ni@PDA. (d) Fluorescence spectra of ZGGO:Ni@PDA and *R. palustris*-ZGGO:Ni@PDA with excitation wavelength of 290 nm (Inset: Normalized photoluminescence intensity versus time after assembly). (e) Lifetime of photoexcited states determined by time-correlated single-photo counting. Lifetimes are presented as the mean values from bi-exponential fittings. (f) Photophysical processes in *R. palustris*-ZGGO:Ni@PDA hybrid system. (g) Log_2 ($NADPH/NADP^+$) in *R. palustris* with or without electron transfer channels represented by "+" and "–" respectively. Data presented as mean values ± SD., $n = 3$. (h) Schematic illustration of the electron transfer channel module facilitating photo-induced charge transfer into *R. palustris*.

that the designed channel enabled efficient electron transfer (Figure S6).

Direct interactions at the R-ZGGO:Ni-microbe interfaces are beneficial for the electron transfer process. SEM mapping of the R-ZGGO:Ni@PDA-microbe hybrid system in Figure 3b clearly shows the PDA encapsulated R-ZGGO:Ni are in close contact with the microorganism, suggesting effective interface self-assembly. The self-assembly between ZGGO:Ni@PDA and *R. palustris* is demonstrated to be driven by van der Waals interaction through the opposite electrostatic potentials (Figure S7). The self-assembly process also demonstrates excellent biocompatibility towards *R. palustris* (Figure S8–S10). Subsequently, the percentage of self-assembled ZGGO:Ni@PDA nanoparticles in the hybrid suspension and the average number of nanoparticles per microbe (N) were quantitatively determined.[9b] Specifically, *R. palustris* cultures were firstly mixed with ZGGO:Ni@PDA at different dilution ratios, followed by filtering the hybrid suspension through a syringe filter with 0.2 μm pore size to leave the free ZGGO:Ni@PDA nanoparticles. The absorbance of the above filtered mixture was then measured. As shown in Figure 3c, a linear relationship between the dilution ratio and 1/N can be clearly observed according to a Langmuir-type adsorption model with the dimensionless equilibrium constant K_{eq} of 1.6×10^2 and a maximum number of 2.2×10^3 adsorbed nanoparticles for one

bacterial cell. The above results indicate that PDA-modified ZGGO:Ni exhibits excellent binding ability towards microbes.

To investigate the capability of the two designed modules in facilitating the electron transfer process, we further investigated the photophysical charge-transfer kinetics at the interfaces of *R. palustris* and ZGGO:Ni@PDA. Upon blending the microorganism with ZGGO:Ni@PDA, we meticulously tracked the temporal dynamics of the maximal photoluminescence intensity within the mixed solution. As illustrated in Figure 3d, ZGGO:Ni@PDA alone demonstrated the most pronounced emission intensity peaking at approximately 700 nm, maintaining a consistent photophysical stability over time. However, upon the introduction of *R. palustris*, there is a notable time-dependent attenuation in the maximal photoluminescence intensity, indicating a dynamic interaction between the photo-induced module and the microorganism (Figure 3d). The results suggest that the assembly of ZGGO:Ni@PDA leads to a rapid transfer of photo-induced charges between ZGGO:Ni@PDA and *R. palustris.* In addition, it can be seen that the average lifetime of the mixed solution decreased from 5.2 μs to 0.5 μs upon the addition of *R. palustris* as shown in Figure 3e (Table S3). Accordingly, the rate constant of charge-transfer between the two modules and microbes (k_{ET}), the rate constants for non-radiative recombination (k_{NR}) and radiative electron-hole recombination (k_{PL}) were calculated (detail in Method section).[9b] It can be found that the calculated k_{ET} value ($1.9\times10^6\ s^{-1}$) is much larger than the total value of k_{NR} and k_{PL} ($k_{NR} + k_{PL} = 1.91\times10^5\ s^{-1}$) (Figure 3f). The above results suggest that the designed two modules could lead to a rapid transfer of photo-induced electrons towards the microbes. Figure 3g demonstrates that the NADPH/$NADP^+$ ratio can be further improved by introducing the designed electron transfer channel module based on PDA, suggesting a more efficient electron transfer process towards *R. palustris.* These above results indicate that our designed electron transfer channel module is promising in facilitating the delivery of reducing power from the photo-induced electron module towards the microbes (Figure 3h).

In addition to the key reducing equivalent of NADPH, ATP is also critical in microbial anabolism. Typically, ATP synthesis is driven by a proton motive force.[8] In natural photosynthesis, the process of electron transfer often involves the concerted movement of a proton, leading to the formation of proton motive force to drive ATP synthesis.[8] Similarly, the capability of the two modules described above to facilitate electron transfer would be promising in maintenance of a microbial transmembrane proton gradient. Furthermore, proteorhodopsins which are light-activated H^+ transporters and can capture green light to generate a proton motive force were introduced for ATP synthesis (Figure S11).[18]

Subsequently, the performance of the proton gradient module in driving "energy currency" (i.e., ATP) production was explored. Non-invasive micro-test technology (denoted as NMT) was adopted to investigate the influence of the designed proton gradient module on H^+ kinetic behavior surrounding the microorganism in real-time (Figure S12).[19] As shown in Figure 4a, it can be observed that the addition of ZGGO:Ni@PDA can further increase the H^+ outflow flux with light irradiation, reaching a 4.9 times higher flux rate of 1.8 pmol $cm^{-2}\ s^{-1}$ at 30 min compared with the ZGGO:Ni@PDA untreated group. Additionally, the NMT curves demonstrate remarkable H^+ outflow trends with light irradiation, while demonstrating H^+ internal flow trends in the dark both in the wild type (WT) and proteorhodopsin-expressed *R. palustris* (Figure 4b), suggesting that the photosynthesis process leads to the effluxion of protons. These results indicate that both the expression of proteorhodopsin and the integration of ZGGO:Ni@PDA facilitate the H^+ outflow (Figure 4b). Considering that H^+ outflow is critical for the formation of the cross-membrane proton gradients to drive ATP synthase and transform ADP and Pi into ATP,[20] we subsequently quantified and compared the ATP concentration in *R. palustris* under different conditions. Expectedly, as shown in Figure 4c, both the integration of the designed light-driven bionic system of ZGGO:Ni@PDA and the expression of proteorhodopsin increase the ATP concentration in *R. palustris* (Figure S13 and S14). The above results indicate that both proteorhodopsin and ZGGO:Ni@PDA drive the proton gradient for ATP generation.

Carbonyl cyanide m-chlorophenyl hydrazone (CCCP) is a lipid-soluble molecule capable of uncoupling the electron transfer from ATP synthesis.[21] In addition, rotenone has been reported as an inhibitor of NADH dehydrogenase capable of blocking electron transfer from the iron-sulfur clusters in NADH dehydrogenase to ubiquinone[21] Both CCCP and rotenone can inhibit the electron transfer process in *R. palustris.*[21] Figure 4d-4e clearly show that upon the addition of CCCP or rotenone, the ATP concentrations in both *R. palustris* cultured with ZGGO:Ni@PDA and bare *R. palustris* decrease. This can be ascribed to the hindered electron transfer processes. Furthermore, upon the addition of CCCP and rotenone, the ATP concentrations in *R. palustris* cultured with ZGGO:Ni@PDA decreased much more obviously compared with the ones in bare *R. palustris.* This can be attributed to the photo-induced electron transfer interception from ZGGO:Ni@PDA to *R. palustris* (Figure S15–S17). Figure 4f shows that upon the addition of the electron shuttle humic acid (HA),[22] ATP concentration are 1.74 times higher in *R. palustris* cultured with ZGGO:Ni@PDA than the bare *R. palustris*, demonstrating that accelerated electron transfer processes increase ATP concentrations (Figure S18 and S19). The above results indicate that electron transfer processes play critical roles in facilitating ATP generation.

Ethylenediaminetetraacetic acid (EDTA) has been reported as an inhibitor for H_2-uptake hydrogenase.[23] As Figure 4g shows, upon the addition of EDTA, ATP concentrations decreased 1.5 times more in *R. palustris* cultured with ZGGO:Ni@PDA compared with the bare *R. palustris* (Figure S20). These results can be attributed to the inhibited reactions between the H_2-uptake hydrogenase and ZGGO:Ni@PDA-produced H_2, thus impacting the proton gradient and ATP generation. Perfluorocarbon nanoemulsions, as suitable H_2 carriers, can accelerate the kinetics of H_2

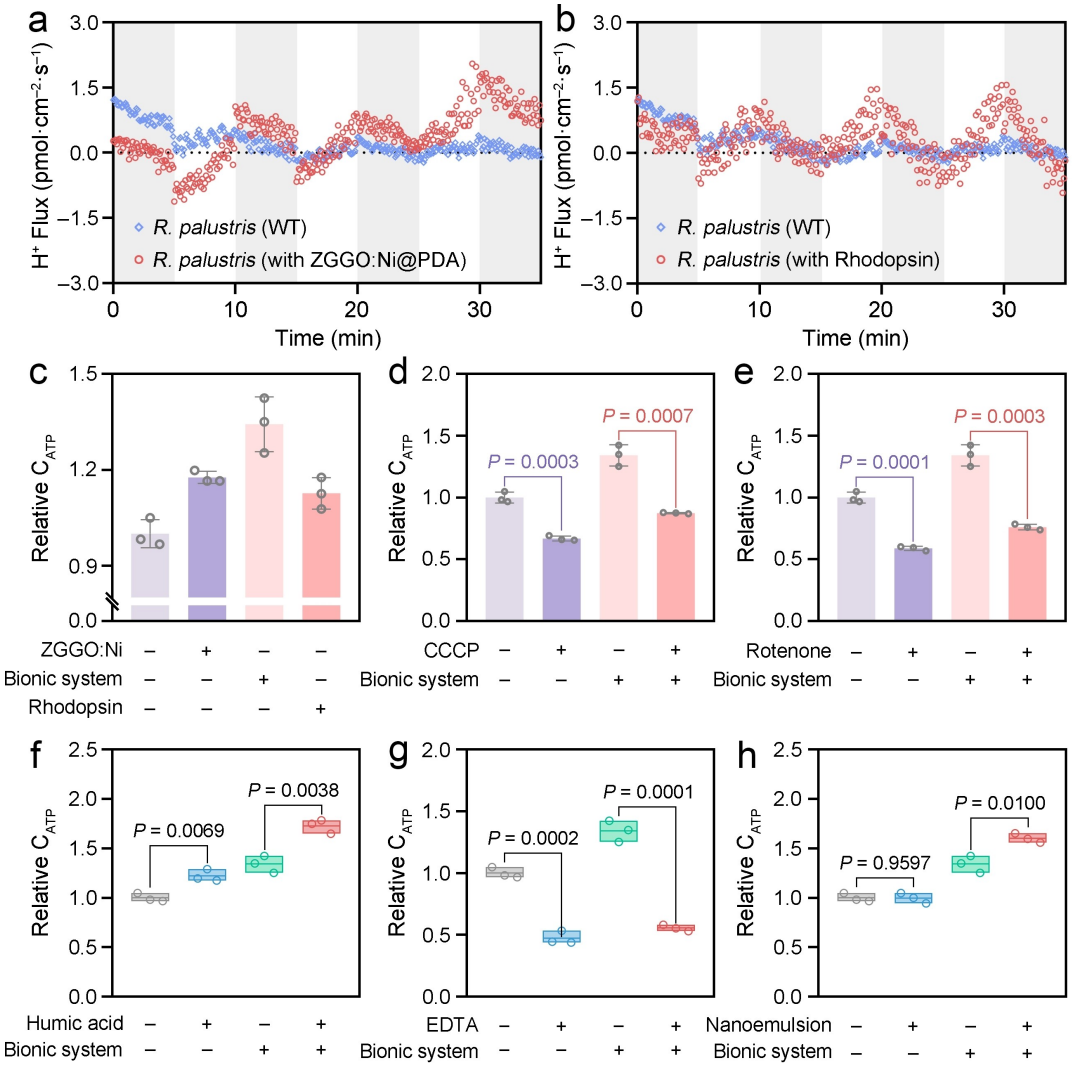

Figure 4. Effect of proton gradient across microbial membrane interface on ATP production. (a) Time-course recording of H^+ oscillation upon integration of the designed light-driven biohybrid photosynthetic system ZGGO:Ni@PDA. (b) Time-course recording of H^+ oscillation in the outer membrane of WT and proteorhodopsin-expressed *R. palustris* during light-dark cycles. (c) ATP concentrations at different conditions. Data presented as mean values ± SD., $n=3$. (d-h) ATP concentration of *R. palustris* upon addition of electron transfer inhibitor CCCP (d), rotenone (e), electron shuttle HA (f), H_2-uptake hydrogenase inhibitor EDTA (g) and nanoemulsion (h). Data presented as mean values ± SD., $n=3$. *P* values were determined by an unpaired two-sided t-test.

delivery and alleviate the throughput constraints.[10b] Figure 4h demonstrates that the ATP concentrations increased upon the addition of such nanoemulsion, further indicating that H_2 impacts microbial ATP metabolism (Figure S21). Overall, the above results validate that the designed light-driven bionic system drives the supply of ATP.

It is widely recognized that NADPH and ATP play critical roles in driving microbial metabolism. Subsequently, we further probed microbial metabolism during photocatalytic fixation of CO_2 and lycopene biosynthesis in *R. palustris* with the designed light-driven bionic system. As shown in Figure 5a and 5b, upon the integration of the designed light-driven bionic system ZGGO:Ni@PDA, CO_2 fixation and lycopene biosynthesis efficiency increased 1.12 and 1.85 times respectively compared with the bare *R. palustris* system, suggesting that the designed NADPH and ATP self-supply light-driven bionic system both facilitates the anabolism metabolism of CBB and MEP pathways. Additionally, the efficiency of CO_2 fixation and lycopene biosynthesis can be further improved by introducing the H^+ pumping proteorhodopsins (Figure S22 and S23). The above results indicate that the designed NADPH and ATP self-supply light-driven bionic system strategy provides a promising way to enable use of photons as energy sources, thus boosting powerful biomanufacturing technology.

To have a comprehensive understanding of the designed light-driven bionic system function mechanism in driving microbial anabolism, transcriptomic analysis was further performed. Genes with significant expression changes were assessed based on the Log_2 (fold change) (Log_2 FC) values. As shown in Figure 5c, of 4535 transcripts detected in *R. palustris*, 769 were significantly associated with the light-

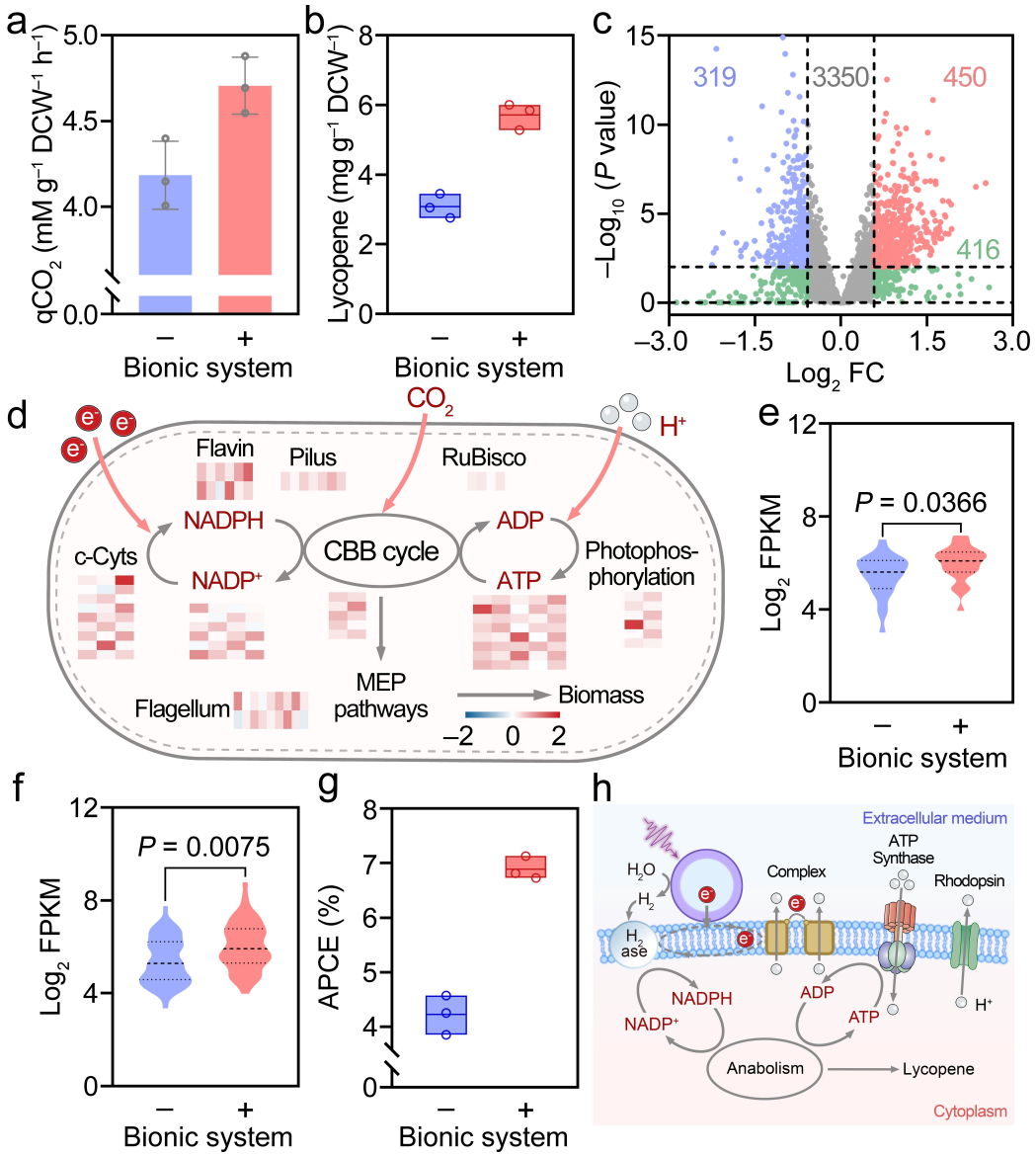

Figure 5. Molecular mechanism of the light-driven bionic system in facilitating microbial anabolism in *R. palustris*. (a) CO_2 fixing rate of *R. palustris*. Data presented as mean values ± SD., $n=3$. (b) Lycopene yields of *R. palustris*. Data presented as mean values ± SD., $n=3$. (c) Volcano plot of differentially expressed genes in *R. palustris*. The threshold of Log_2 FC is $|0.58|$ (i.e., FC $\geq |1.5|$), and that of *P* value is <0.05. There were 769 differentially expressed microbial transcripts that met these criteria. (d) Schematic illustration of ZGGO:Ni@PDA driving lycopene synthesis and CO_2 fixation. Inset heat maps showing the differential gene expression presented as Log_2 FC value. (e-f) Violin plots showing the significant differences in expression of (e) reducing equivalent related genes and (f) ATP related genes of *R. palustris*. (g) APCE value with light-driven bionic system. Data presented as mean values ± SD., $n=3$. (h) Schematic illustration of light-driven bionic system facilitating microbial anabolism.

driven bionic system ZGGO:Ni@PDA (*P* value <0.05 and FC $\geq |1.5|$), indicating that ZGGO:Ni@PDA influences the gene expressions of the microorganism. This is shown in Figure 5d, which presents the overrepresented (white to red) and underrepresented transcript (white to blue) with the reference to gene expressions in bare *R. palustris* without ZGGO:Ni@PDA (Figure 5d). The Log_2 FC values of electron transfer proteins, including flagellum, pilus, c-type cytochromes (c-Cyts), H_2-uptake PioABC and complex hydrogenase are greater than 0 on the whole (Figure S24), indicating that genes encoding electron transfer proteins are actively expressed upon the integration of ZGGO:Ni@PDA. The results suggest that the designed light-driven bionic system ZGGO:Ni@PDA can facilitate microbial metabolism by promoting the expression of proteins associated with electron transport. Additionally, it was found that the reducing power NADPH and critical energy ATP associated genes had higher expression levels represented as Log_2 FPKM (fragments per kilobase per million mapped reads) values upon the addition of the designed light-driven bionic system ZGGO:Ni@PDA (Figure 5e,f). Moreover, by integrating the designed NADPH and ATP self-supply light-driven bionic system, the photon conversion efficiency improved 1.6 times reaching 6.9 % (Figure 5g). The energy

conversion efficiency of the bionic system significantly surpasses that of its predecessors both in vivo and in vitro biosynthesis systems,[24] further underscoring the merits of the bionic system proposed in this study (Table S4). Collectively, the above results affirm that the highly efficient light-driven bionic system facilitates microbial anabolism through facilatating the NADPH and ATP production with the aid of electron transfer associated proteins and hydrogenase (Figure 5h, Figure S25–S29).

Furthermore, to broaden our understanding of the photosynthesis-derived bionic system's applications, we have extended our investigation to assess the system's performances in basal inorganic culture medium and with model strains of *Escherichia coli* (*E. Coli*). As shown in Figure S30, it is evident that the lycopene biosynthesis efficiency in the bionic system has increased 2.4 times when compared to the bare *R. palustris* in the basal medium.[25] Additionally, upon applying the bionic system to the engineered *E. Coli* model strain,[7a] which is designed for the biosynthesis of jet fuel farnesene and features genetically encoded fluorescent indicators for NADPH (iNap sensors),[26] it can be observed that both the NADPH content and the farnesene yield experienced an increase (Figure S31 and S32). Collectively, the aforementioned results provide further validation of the versatility and applicability of our proposed bionic system.

Conclusion

In conclusion, we introduced a pioneering light-driven bionic platform that seamlessly integrates three critical modules: the photo-induced electron module, the electron transfer channel module and the proton gradient module for the simultaneous and controllable supply of NADPH and ATP to achieve highly efficient CO_2 fixation and biomanufacturing.The designed NADPH and ATP self-supply light-driven bionic system strategy enables for microbial metabolism regulation with light sources. In contrast to the previously reported biohybrid systems that have focused on developing advanced materials with high efficiency in terms of biocompatibility and electron transfer efficiency,[9b,d,10a,11a] this study not only introduces a novel advanced material but also provides unique perspectives on the design of biohybrids. Our proposed biohybrid design strategy, which integrates three pivotal modules to achieve the simultaneous and controlled supply of NADPH and ATP, presents novel insights and opportunities that could revolutionize CO_2 fixation and biomanufacturing technology. In a broader context, with the boosting development of synthetic biology, our light-driven bionic system strategy here can be easily extended to produce other high value-added products, opening new doors for the sustainable biomanufacturing industry. In our subsequent work, we will continue to focus on channeling the critical NADPH and ATP specifically into the desired pathways for higher target chemical production and improving the tolerance of bionic platforms for practical large-scale fermentation.

Acknowledgements

This work is supported by the National Natural Science Foundation of China (21925401, 52221001 to Q.Y.), the National Key R&D Program of China (2023YFF1205900 to Q.Y.), the Fundamental Research Funds for the Central Universities (2042022rc0004 to Q.Y), Hunan Provincial Key Research and Development Plan (2024JK2117 to Q.Y.), "Sharp Knife" Technology Research Program of Hubei Province (2023BAA002 to Q.Y), China Postdoctoral Science Foundation (2024 M752456 to C.N), Postdoctoral Innovative Research of Hubei Province of China (211000025 to C.N), Youth Talent Program of Sci-Tech Think Tank (XMSB20240710060 to C.N), New Cornerstone Science Foundation through the XPLORER PRIZE, Interdisciplinary Innovative Talents Foundation from Renmin Hospital of Wuhan University. We thank the Core Facility of Wuhan University for SEM, TEM and GC-MS analysis. We thank Dr. Jing Xu of the Core Facility of Wuhan University for the testing service. We also thank Professor Liming Liu's group and Professor Yi Yang's group for providing Rhodopsin expressed and iNap expressed plasmids respectively.

Conflict of Interest

The authors declare no conflict of interest.

Data Availability Statement

The data that support the findings of this study are available in the supplementary material of this article.

Keywords: bionic system · sustainable biosynthesis · CO_2 fixation · NADPH · ATP

[1] a) S. Luo, P. P. Lin, L. Nieh, G. Liao, P. W. Tang, C. Chen, J. C. Liao, *Nat. Catal.* **2022**, *5*, 154–162; b) Hu, G. P., Li, Y., Ye, C., Liu, L. M., Chen, X. L. *Trends in Biotechnol.* **2019**, *37*, 532–547.

[2] a) R. Cavicchioli, W. J. Ripple, K. N. Timmis, F. Azam, L. R. Bakken, M. Baylis, M. J. Behrenfeld, A. Boetius, P. W. Boyd, A. T. Classen, T. W. Crowther, R. Danovaro, C. M. Foreman, J. Huisman, D. A. Hutchins, J. K. Jansson, D. M. Karl, B. Koskella, D. B. M. Welch, J. B. H. Martiny, M. A. Moran, V. J. Orphan, D. S. Reay, J. V. Remais, V. I. Rich, B. K. Singh, L. Y. Stein, F. J. Stewart, M. B. Sullivan, M. J. H. Oppen, S. C. Weaver, E. A. Webb, N. S. Webster, *Nat. Rev. Microbiol.* **2019**, *17*, 569–586; b) D. Y. Li, H. Dong, X. P. Cao, W. Y. Wang, C. Li, *Nat. Commun.* **2023**, *14*, 5337.

[3] a) Q. Wang, S. Kalathil, C. Pornrungroj, C. D. Sahm, E. Reisner, *Nat. Catal.* **2022**, *5*, 633–641; b) N. J. Claassens, D. Z. Sousa, V. A. P. M. Santos, W. M. Vos, Oost van der, *Nat. Rev. Microbiol.* **2016**, *14*, 692–706; c) X. Fang, S. Kalathil, E. Reisner, *Chem. Soc. Rev.* **2020**, *49*, 4926–4952; d) R. T. Zhang, Y. He, J. Yi, L. J. Zhang, C. P. Shen, S. J. Liu, L. F. Liu, B. H. Liu, L. Qiao, *Chem* **2020**, *6*, 234–249.

[4] a) T. T. Zheng, M. Zhang, L. Wu, S. Guo, X. Liu, J. Zhao, W. Xue, J. Li, C. Liu, X. Li, Q. Jiang, J. Bao, J. Zeng, T. Yu, C.

Xia, *Nat. Catal.* **2022**, *5*, 388–396; b) S. Atsumi, W. Higashide, J. C. Liao, *Nat. Biotechnol.* **2009**, *27*, 1177–1180.
[5] a) H. M. Woo, *Curr. Opin. Biotechnol.* **2017**, *45*, 1–7; b) P. Zhu, X. L. Chen, *Chem* **2022**, *8*, 1178–1180; c) J. D. Keasling, *Nature* **2012**, *492*, 13; d) J. Ni, H. Y. Liu, F. Tao, Y. T. Wu, P. Xu, *Angew. Chem. Int. Ed.* **2018**, *57*, 15990–15994.
[6] a) J. Zhou, F. L. Zhang, H. K. Meng, Y. P. Zhang, Y. Li, *Metab. Eng.* **2016**, *38*, 217–227; b) P. Chen, X. Liu, C. Gu, P. Zhong, N. Song, M. Li, Z. Dai, X. Fang, Z. Liu, J. Zhang, R. Tang, S. Fan, X. Lin, *Nature* **2022**, *612*, 546–554; c) T. Yu, Q. Liu, X. Wang, X. Liu, Y. Chen, J. Nielsen, *Nat. Metab.* **2022**, *4*, 1551–1559; d) F. Gao, G. Y. Liu, A. Chen, Y. G. Hu, H. H. Wang, J. Y. Pan, J. L. Feng, H. W. Zhang, Y. J. Wang, Y. Z. Min, C. Gao, Y. J. Xiong, *Nat. Commun.* **2023**, *14*, 6783.
[7] a) J. Wang, N. Chen, G. Bian, X. Mu, N. Du, W. Wang, C. Ma, S. Fu, B. Huang, T. Liu, Y. Yang, Q. Yuan, *Angew. Chem. Int. Ed.* **2022**, *61*, e202207132; b) G. Hu, Z. Li, D. Ma, C. Ye, L. Zhang, C. Gao, L. Liu, X. Chen, *Nat. Catal.* **2021**, *4*, 395–406.
[8] a) T. Shikanai, H. Yamamoto, *Mol. Plant* **2017**, *10*, 20–29; b) Y. Munekaga, M. Hashimoto, C. Miyake, K. Tomizawa, T. Endo, M. Tasaka, T. Shikanai, *Nature* **2004**, *429*, 579–582; c) B. Y. Yang, S. B. Li, W. Mu, Z. Wang, X. J. Han, *Small* **2023**, *19*, 2201305.
[9] a) S. Berhanu, T. Ueda, Y. Kuruma, *Nat. Commun.* **2019**, *10*, 1325; b) X. Guan, S. Erşan, X. Hu, T. L. Atallah, Y. Xie, S. Lu, B. Cao, J. Sun, K. Wu, Y. Huang, X. Duan, J. R. Caram, Y. Yu, J. O. Park, C. Liu, *Nat. Catal.* **2022**, *5*, 1019–1029; c) K. K. Sakimoto, S. J. Zhang, P. D. Yang, *Nano Lett.* **2016**, *16*, 5883–5887; d) H. Zhang, H. Liu, Z. Tian, D. Lu, Y. Yu, C. Stefano, K. K. Sakimoto, P. D. Yang, *Nat. Nanotechnol.* **2018**, *13*, 900–905; e) R. Zhang, Y. He, J. Yi, L. Zhang, C. Shen, S. Liu, L. Liu, B. Liu, L. Qiao, *Chem.* **2020**, *6*, 234–249; f) J. Guo, M. Suástegui, K. K. Sakimoto, V. M. Moody, G. Xiao, D. G. Nocera, N. S. Joshi, *Science* **2018**, *362*, 813–816.
[10] a) S. Cestellos-Blanco, H. Zhang, J. M. Kim, Y. X. Shen, P. D. Yang, *Nat. Catal.* **2020**, *3*, 245–255; b) S. Lu, R. M. Rodrigues, S. Huang, D. A. Estabrook, J. O. Chapman, X. Guan, E. M. Sletten, C. Liu, *Chem. Catal.* **2021**, *1*, 704–720; c) J. Ye, C. Wang, C. Gao, T. Fu, C. H. Yang, G. P. Ren, J. Lv, S. G. Zhou, Y. J. Xiong, *Nat. Commun.* **2022**, *13*, 6612.
[11] a) C. Liu, B. C. Colon, M. Ziesack, P. A. Silver, D. G. Nocera, *Science* **2016**, *352*, 1210–1213; b) K. K. Sakimoto, N. Kornienko, S. Cestellos-Blanco, J. Lim, C. Liu, P. D. Yang, *J. Am. Chem. Soc.* **2018**, *140*, 1978–1985; c) W. Yu, Y. Zeng, Z. Wang, S. Xia, Z. Yang, W. Chen, Y. Huang, F. Lv, H. Bai, S. Wang, *Sci. Adv.* **2023**, *9*, eadf6772; d) X. Zhou, Y. Zeng, Y. Tang, Y. Huang, F. Lv, L. Liu, S. Wang, *Sci. Adv.* **2020**, *6*, eabc5237; e) Z. Chen, G. Quek, J. Zhu, S. J. W. Chan, S. J. Cox-Vázquez, F. Lopez-Garcia, G. C. Bazan, *Angew. Chem. Int. Ed.* **2023**, *135*, e202307101.
[12] a) L. Xu, Y. Zhao, K. A. Owusu, Z. Zhuang, Q. Liu, Z. Wang, Z. Li, L. Mai, *Chem.* **2018**, *4*, 1538–1559; b) F. Guo, J. Chen, J. Zhao, Z. Chen, D. Xia, Z. Zhan, Q. Wang, *Chem. Eng. J.* **2020**, *386*, 124014; c) Y. Kim, E. Coy, H. Kim, R. Mrówczyński, P. Torruella, D. Jeong, K. S. Choi, J. H. Jang, M. Y. Song, D. Jang, F. Peiro, S. Jurga, H. J. Kim, *Appl. Catal. B* **2021**, *280*, 119423; d) Y. Y. Yu, Y. Z. Wang, Z. Fang, Y. T. Shi, Q. W. Cheng, Y. X. Chen, W. Shi, Y. C. Yong, *Nat. Commun.* **2020**, *11*, 4087; e) S. Y. Park, H. Eun, M. H. Lee, S. Y. Lee, *Nat. Catal.* **2022**, *5*, 726–737.
[13] a) S. Wang, X. Hai, X. Ding, S. Jin, Y. Xiang, P. Wang, B. Jiang, F. Ichihara, M. Oshikiri, X. Meng, Y. Li, W. Matsuda, J. Ma, S. Seki, X. Wang, H. Huang, Y. Wada, H. Chen, J. Ye, *Nat. Commun.* **2020**, *11*, 1149; b) J. Guo, B. L. Tardy, A. J. Christofferson, Y. Dai, J. J. Richardson, W. Zhu, M. Hu, Y. Ju, J. Cui, R. R. Dagastine, I. Yarovsky, F. Caruso, *Nat. Nanotechnol.* **2016**, *11*, 1105–1111.
[14] G. L. Li, J. B. Fei, Y. Q. Xu, B. B. Sun, J. B. Li, *Angew. Chem. Int. Ed.* **2019**, *58*, 1110–1114.
[15] Z. Zafar, S. Yi, J. Li, C. Li, Y. Zhu, A. Zada, W. Yao, Z. Liu, X. Yue, *Energy Environ. Mater.* **2022**, *5*, 68–114.
[16] X. Xu, J. Ren, G. Chen, D. Kong, C. Gu, C. Chen, L. Kong, *Opt. Mater. Express* **2013**, *3*, 10.
[17] J. Wang, N. Chen, W. Wang, Z. Li, B. Huang, Y. Yang, Q. Yuan, *CCS Chem.* **2023**, *5*, 164–175.
[18] a) N. J. Claassens, M. Volpers, V. A. P. M. Santos, J. van der Oost, W. M. de Vos, *Trends in Biotechnol.* **2013**, *31*, 633–642; b) W. Tu, W. E. Huang, *Environ. Microbiol.* **2022**, *25*, 126–130; c) C. Engelhard, I. Chizhov, F. Siebert, M. Engelhard, *Chem. Rev.* **2018**, *118*, 10629–10645.
[19] a) B. H. Liu, J. H. Zhang, N. H. Ye, *Trends in Plant Sci.* **2023**, *28*, 123–124; b) J. Meng, L. Liang, P. Jia, Y. Wang, H. Li, W. Yang, *Nat. Plants* **2020**, *6*, 143–153.
[20] X. Xu, J. Fei, Y. Xu, G. Li, W. Dong, H. Xue, J. Li, *Angew. Chem. Int. Ed.* **2021**, *60*, 7617–7620.
[21] a) N. Chen, N. Du, R. Shen, T. He, J. Xi, J. Tan, G. Bian, Y. Yang, T. Liu, W. Tan, L. Yu, Q. Yuan, *Nat. Commun.* **2023**, *14*, 6800; b) M. S. Guzman, K. Rengasamy, M. M. Binkley, C. Jones, T. O. Ranaivoarisoa, R. Singh, D. A. Fike, J. M. Meacham, A. Bose, *Nat. Commun.* **2019**, *10*, 1355.
[22] H. Zuo, R. Kukkadapu, Z. Zhu, S. Ni, L. Huang, Q. Zeng, C. Liu, H. Dong, *Sci. Total Environ.* **2020**, *741*, 140213.
[23] J. Fiβler, C. Schirra, G. W. Kohring, F. Giffhorn, *Appl. Microbiol. Biotechnol.* **1994**, *41*, 395–399.
[24] a) F. Li, X. L. Wei, L. Zhang, C. Liu, C. You, Z. G. Zhu, *Angew. Chem. Int. Ed.* **2022**, *61*, e202111054; b) T. E. Miller, T. Beneyton, T. Schwander, C. Diehl, M. Girault, R. McLean, T. Chotel, P. Claus, *Science* **2020**, *368*, 649–654.
[25] a) M. T. Madigan, H. Gest, *FEMS Microbiol. Ecol.* **1988**, *53*, 53–58; b) H. Gest, J. L. Favinger, M. T. Madigan, *FEMS Microbiol. Ecol.* **1985**, *31*, 317–322.
[26] R. K. Tao, Y. Z. Zhao, H. Y. Chu, A. Wang, J. H. Zhu, X. J. Chen, Y. J. Zou, M. Shi, R. M. Liu, N. Su, J. L. Du, H. M. Zhou, L. Y. Zhu, X. H. Qian, H. Y. Liu, J. Losclzo, Y. Yang, *Nat. Methods* **2017**, *14*, 720–728.

Manuscript received: August 7, 2024
Accepted manuscript online: January 13, 2025
Version of record online: January 21, 2025